HHS Public Access

Author manuscript

Sci Transl Med. Author manuscript; available in PMC 2020 December 21.

Published in final edited form as:

Sci Transl Med. 2020 August 05; 12(555): . doi:10.1126/scitranslmed.aay1371.

Glycolysis links reciprocal activation of myeloid cells and endothelial cells in the retinal angiogenic niche

Zhiping Liu[1,2], **Jiean Xu**[1,2], **Qian Ma**[2], **Xiaoyu Zhang**[2], **Qiuhua Yang**[2], **Lina Wang**[2], **Yapeng Cao**[2], **Zhimin Xu**[2], **Amany Tawfik**[3,4], **Ye Sun**[5], **Neal L. Weintraub**[2], **David J. Fulton**[2], **Mei Hong**[1,6], **Zheng Dong**[7,8], **Lois E. H. Smith**[5], **Ruth B. Caldwell**[2,4,7,8,*], **Akrit Sodhi**[9], **Yuqing Huo**[2,4,7,*,†]

[1]State Key Laboratory of Chemical Oncogenomics, Key Laboratory of Chemical Genomics, School of Chemical Biology and Biotechnology, Peking University Shenzhen Graduate School, Shenzhen 518055, China

[2]Vascular Biology Center, Medical College of Georgia, Augusta University, Augusta, GA 30912, USA

[3]Department of Oral Biology and Anatomy, Dental College of Georgia, Augusta University, Augusta, GA 30912, USA

[4]James and Jean Culver Vision Discovery Institute, Medical College of Georgia, Augusta University, Augusta, GA 30912, USA

[5]Department of Ophthalmology, Boston Children's Hospital, Harvard Medical School, Boston, MA 02115, USA

[6]Shenzhen-Hong Kong Institute of Brain Science-Shenzhen Fundamental Research Institutions, Shenzhen 518055, China

[7]Department of Cellular Biology and Anatomy, Medical College of Georgia, Augusta University, Augusta, GA 30912, USA

[8]Charlie Norwood Veterans Affairs Medical Center, Augusta, GA 30912, USA

[9]Wilmer Eye Institute, Johns Hopkins School of Medicine, Baltimore, MD 21287, USA

Abstract

[†]Corresponding author. yhuo@augusta.edu.
[*]These authors contributed equally to this work as co-senior authors.

Author contributions: Z.L., R.B.C., and Y.H. designed the study. Z.L. and J.X. performed flow cytometry analysis. Z.L. and Q.M. performed aortic spouting assay. Q.Y. performed isolation, culture, and identification of MAECs. Z.L. and Y.S. performed laser culture microdissection. Z.L., X.Z., L.W., Y.C., A.T., and Z.X. generated the murine models. Z.L. performed the remainder of imaging and data collection. Z.L., J.X., R.B.C., and Y.H. analyzed the data. Z.L. and Y.H. wrote the manuscript. N.L.W., D.J.F., L.E.H.S., R.B.C., and A.S. critically reviewed and revised the manuscript. Z.L., R.B.C., M.H., L.E.H.S., Z.D., A.S., Y.S., and Y.H. provided the reagents or materials and participated in designing the experiments.

SUPPLEMENTARY MATERIALS
stm.sciencemag.org/cgi/content/full/12/555/eaay1371/DCl

Competing interests: The authors declare that they have no competing interests.

Data and materials availability: All data associated with this study are present in the paper or the Supplementary Materials.

The coordination of metabolic signals among different cellular components in pathological retinal angiogenesis is poorly understood. Here, we showed that in the pathological angiogenic vascular niche, retinal myeloid cells, particularly macrophages/microglia that are spatially adjacent to endothelial cells (ECs), are highly glycolytic. We refer to these macrophages/microglia that exhibit a unique angiogenic phenotype with increased expression of both M1 and M2 markers and enhanced production of both proinflammatory and proangiogenic cytokines as pathological retinal angiogenesis–associated glycolytic macrophages/microglia (PRAGMs). The phenotype of PRAGMs was recapitulated in bone marrow–derived macrophages or retinal microglia stimulated by lactate that was produced by hypoxic retinal ECs. Knockout of 6-phosphofructo-2-kinase/fructose-2, 6-bisphosphatase (*PFKFB3*; *Pfkfb3* for rodents), a glycolytic activator in myeloid cells, impaired the ability of macrophages/microglia to acquire an angiogenic phenotype, rendering them unable to promote EC proliferation and sprouting and pathological neovascularization in a mouse model of oxygen-induced proliferative retinopathy. Mechanistically, hyperglycolytic macrophages/microglia produced large amount of acetyl–coenzyme A, leading to histone acetylation and PRAGM-related gene induction, thus reprogramming macrophages/microglia into an angiogenic phenotype. These findings reveal a critical role of glycolytic metabolites as initiators of reciprocal activation of macrophages/microglia and ECs in the retinal angiogenic niche and suggest that strategies targeting the metabolic communication between these cell types may be efficacious in the treatment of pathological retinal angiogenesis.

INTRODUCTION

Pathological angiogenesis is a major cause of irreversible blindness in individuals of all age groups (1–4). Increased endothelial sprouting and proliferation are major cellular events that underlie pathological angiogenesis, and endothelial glycolysis has been demonstrated to be the principal metabolic source to support these cellular events. We and others have previously demonstrated that glycolysis is critical for the sprouting of tip endothelial cells (ECs) and the proliferation of stalk cells in zebrafish and that mice deficient in the glycolytic activator 6-phosphofructo-2-kinase/fructose-2, 6-bisphosphatase (*PFKFB3*; *Pfkfb3* for rodents) have impaired angiogenesis (5, 6). Deficiency of endothelial *Pfkfb3* in mice has also been reported to reduce pathological angiogenesis in models of retinopathy of prematurity and age-related macular degeneration (AMD) (6, 7). However, the mechanisms that trigger the up-regulation of endothelial glycolysis or enhance glycolysis in adjacent cells, such as macrophages/microglia, in the angiogenic vascular niche, as well as the factors that mediate metabolic cross-talk between ECs and their neighboring cells remain unknown.

Macrophages/microglia within neovascular areas contribute to aberrant angiogenesis (8–11). However, the phenotype and metabolic states of macrophages/microglia that contribute to pathological retinal angiogenesis remain unclear. Macrophages/microglia are highly plastic and can acquire a range of functional phenotypes, including that of the classically activated state (M1) and the alternatively activated state (M2), in response to various stimuli in the local microenvironment (12, 13). A prominent population of tumor-associated macrophages, for example, undergoes alternative activation in the tumor microenvironment and expresses M2-associated genes and angiogenic factors, such as arginase-1 (*Arg1*) and vascular endothelial growth factor (*Vegf*), to promote angiogenesis and fuel cancer progression (14,

15). Likewise, M2 macrophages/microglia are also considered to be the predominant myeloid cells in the development of both retinal and choroidal neovascularization (16, 17). In addition, proinflammatory macrophages, which express proinflammatory cytokines such as interleukin-1β (IL-1β) and tumor necrosis factor-α, are reported to be critical for pathological retinal angiogenesis (18). Thus, the exact phenotype of the myeloid cells driving angiogenesis remains incompletely defined. Moreover, recent studies show that both classic and alternatively activated macrophages are critically supported by metabolic changes, especially increased glycolytic reprogramming (19, 20). Various stimuli in the microenvironment can alter macrophage metabolism and subsequently regulate the expression of genetic programs that shape macrophage phenotype and function (19, 20). The metabolic changes that support the altered phenotype of macrophages/microglia in retinal angiogenesis remain undetermined.

The regulatory effects of glucose or glycolytic metabolism on macrophage function have been only partially explored. Distinct metabolic shifts in macrophages can polarize and activate macrophages through the manipulation of several unique metabolites including lactate and succinate (21, 22). In pluripotent stem cells, increased glycolysis enhances the formation of acetyl–coenzyme A (Ac-CoA), a substrate critical for the acetylation of proteins, including histones, and a regulator of stem cell fate (23–27). Thus far, it has not been defined whether and how glycolysis and histone acetylation are coordinated to influence the specific gene expression profile that underlies macrophage/microglia activation in pathological retinal angiogenesis.

In the current study, we explored the role and mechanism of metabolic cross-talk between a population of hyperglycolytic proangiogenic macrophages/microglia that we have termed pathological retinal angiogenesis–associated glycolytic macrophages/microglia (PRAGMs) and retinal ECs (RECs) in the angiogenic niche.

RESULTS

Retinal macrophages/microglia adjacent to ECs are hyperglycolytic in the pathological angiogenic vascular niche

Mouse neonatal retinas and retinas of oxygen-induced proliferative retinopathy (OIR) are well-accepted models for studying retinal angiogenesis (Fig. 1A) (28). Using these models, we examined the spatial relationship between macrophages/microglia and the retinal vasculature to assess the contribution of EC-macrophage/microglia cross-talk to retinal angiogenesis. During the development of the retinal vasculature, macrophages/microglia can be found embracing the outside of the blood vessel wall (Fig. 1B) (9, 10, 29) or localized proximal to endothelial tip cells at the leading edge (Fig. 1C), which is consistent with the findings of others (9, 10, 29). In contrast, in OIR retinas, macrophages/microglia accumulate in and around areas of pathological retinal neovascular tufts (Fig. 1D). The identities of these cells were confirmed by immunofluorescence staining of the endothelial nuclear marker, erythroblast transformation-specific (ETS)–related gene (30, 31), isolectin B4, and myeloid F4/80 marker (fig. S1A). Images of the three-dimensional surface generated by confocal *z*-stacks of flat-mounted OIR retinas further revealed that ionized calcium-binding adapter molecule 1 $(IBa1)^+$ macrophages/microglia were localized proximal to $CD31^+$

vascular ECs in the pathological angiogenic niche (Fig. 1E). Collectively, these observations suggest a possible role of endothelial-myeloid interactions in pathological retinal angiogenesis.

Both macrophages/microglia and ECs use glycolysis as their major metabolic pathway (fig. S1B) (5, 20, 32–34). In mouse retinas, the mRNA expression of genes encoding glycolytic enzymes or regulators (fig. S1C) and the amount of lactate (Fig. 1F), the major metabolite of glycolysis, were higher in mice with OIR than in mice maintained in room air (RA). Specifically, a marked increase in the mRNA expression of Pfkfb3, the most potent stimulator of glycolysis (35), was detected in OIR retinas along with an increased amount of its enzymatic product, fructose 2,6-bisphosphate (F-2,6-P2) (fig. S1C). To further elucidate the specific changes in gene expression pattern within the pathological angiogenic niche, we used laser capture microdissection to excise neovascular tufts from postnatal day 17 (P17) OIR retinas (Fig. 1G). Expression of several glycolytic genes was increased in isolated pathological neovascular tufts from OIR mice as compared to those in the normal retinal vasculature from RA mice (Fig. 1H). To examine the expression of glycolytic genes specifically in the macrophages/microglia and ECs of these retinas, we used F4/80 or CD31 antibody–conjugated magnetic beads to isolate mouse retinal macrophages/microglia or ECs, respectively, from OIR and control mice. The mRNA expression of some glycolytic genes and the amount of intracellular lactate were higher in macrophages/microglia and ECs isolated from OIR retinas than in cells obtained from control retinas (Fig. 1, I and J, and fig. S1, D and E). Macrophages/microglia from OIR retinas exhibited a robust increase in *Pfkfb3* mRNA expression (~8-fold higher versus RA) as compared to macrophages/microglia from RA retinas, whereas mRNA expression of *Pfkfb1*, *Pfkfb2*, and *Pfkfb4* was changed only modestly (Fig. 1I). Using multiple immunofluorescence staining of whole-mounted retinas with a knockout (KO)–validated, highly specific monoclonal antibody for Pfkfb3 (33, 36), we observed increased expression of Pfkfb3 in the macrophages/microglia of OIR retinas (Fig. 1, K and L). In addition, higher expression of Glut1 and Pkm2 were also observed in macrophages/microglia of OIR retinas versus macrophages/microglia of control retinas (fig. S1, F to I). Collectively, these findings suggest that glycolysis is increased in both retinal macrophages/microglia and ECs in pathologic retinal angiogenesis.

Myeloid KO of *Pfkfb3* delays vascular development in mouse retinas

To determine the contribution of Pfkfb3-mediated glycolysis in macrophages/microglia to retinal angiogenesis, we generated myeloid-specific *Pfkfb3* KO mice ($Pfkfb3^{\Delta M\phi}$) and control mice ($Pfkfb3^{WT}$) by intercrossing *Lysm*-Cre mice with $Pfkfb3^{flox/flox}$ mice (fig. S2A) (6). Pfkfb3 expression was barely detectable in bone marrow–derived macrophages (BMDMs) cultured with the bone marrow of $Pfkfb3^{\Delta M\phi}$ mice as compared to those of $Pfkfb3^{WT}$ mice (fig. S2, B to D). Pfkfb3 expression was also markedly reduced in macrophages/microglia from retinas of $Pfkfb3^{\Delta M\phi}$ mice (Fig. 2, L to N), confirming effective deletion of *Pfkfb3* in the myeloid cells of $Pfkfb3^{\Delta M\phi}$ mice. Metabolic analysis revealed suppressed pyruvate and lactate production in *Pfkfb3*-deficient BMDMs (fig. S2, E to G), suggesting a key role of Pfkfb3 in regulating macrophage glycolysis. Using the Seahorse extracellular flux analyzer, we assessed glycolytic function of *Pfkfb3*-deficient macrophages by directly measuring the extracellular acidification rate. As shown in fig. S2

(H to K), *Pfkfb3*-deficient BMDMs demonstrated reduced glucose-induced glycolysis but no change in mitochondrial respiratory activity as compared to wild-type (WT) macrophages.

To examine the role of *Pfkfb3* in regulating macrophage/microglia glycolysis in retinal angiogenesis, we first characterized vascular development in the retinas of $Pfkfb3^{\Delta M\phi}$ mice. On P3, the area of vascularized retina was approximately 39% less in $Pfkfb3^{\Delta M\phi}$ mice as compared with that seen in littermate $Pfkfb3^{WT}$ mice (Fig. 2, A and B). Delayed vascular development in the $Pfkfb3^{\Delta M\phi}$ retina was also observed at P5 and P7 (Fig. 2, C to F). At the leading edge of the developing vasculature in $Pfkfb3^{\Delta M\phi}$ retinas at P5, branching and the number of vascular sprouting tips and filopodia were reduced compared with those of littermates (Fig. 2, G to M). Quantitative analysis of blood vessel densities showed that vascularization within the three layers of the retina was suppressed in $Pfkfb3^{\Delta M\phi}$ mice as compared with that of $Pfkfb3^{WT}$ mice at P12, but this difference was lost at P17 (fig. S3, A to D). One month after birth, the retinal vasculature was comparable between $Pfkfb3^{\Delta M\phi}$ and $Pfkfb3^{WT}$ mice (fig. S3, E to I). These results suggest that macrophage/microglia Pfkfb3 contributes to early vascular development but is not essential for the vascularization of retinas in adult mice.

Vascular development is a balance between vascularization and vessel remodeling and regression. Therefore, we next evaluated changes in remodeling and regression of the retinal vasculature to assess whether they contribute to the normalization of the retinal vasculature in adult $Pfkfb3^{\Delta M\phi}$ mice. We quantified the number of collagen IV^+ isolectin $IB4^-$ empty sleeves in the superficial plexus of $Pfkfb3^{\Delta M\phi}$ retinas and found that the number of regressing, acellular capillaries was decreased in $Pfkfb3^{\Delta M\phi}$ retinas (Fig. 2, N and O). These results suggest that the delayed and incomplete retinal vasculature seen in $Pfkfb3^{\Delta M\phi}$ mice during the early stages of retinal development are compensated for by a decrease in vessel pruning and remodeling at later stages.

Myeloid KO of *Pfkfb3* or *Pkm2* suppresses pathological retinal angiogenesis

To assess the role of macrophage/microglia glycolysis in the formation of pathological retinal neovascularization, we induced OIR in WT and $Pfkfb3^{\Delta M\phi}$ mice. After 5 days of hyperoxia, retinal vascular regression at P12 did not show difference in the areas of vaso-obliteration between $Pfkfb3^{\Delta M\phi}$ and $Pfkfb3^{WT}$ mice (fig. S4, A and B). However, by P17, we observed a significant decrease in the area of neovascular tufts in retinas of $Pfkfb3^{\Delta M\phi}$ mice as compared with that in the WT retinas ($P < 0.001$; Fig. 3, A and B). In addition, we also found a decrease in the avascular area in retinas of $Pfkfb3^{\Delta M\phi}$ mice compared with that of $Pfkfb3^{WT}$ mice (Fig. 3C). Retinas of $Pfkfb3^{\Delta M\phi}$ mice also displayed milder hemorrhages compared to controls (fig. S4C). Fluorescein angiography with Alexa Fluor 594–conjugated isolectin B4 and fluorescein isothiocyanate–dextran demonstrated reduced retinal vascular permeability in $Pfkfb3^{\Delta M\phi}$ mice as compared to controls (fig. S4D).

To further establish the role of macrophage/microglia glycolysis in retinal angiogenesis, we next examined OIR in mice deficient in macrophage/microglia *Pkm2*, a critical regulator of the glycolytic reprogramming in macrophages (34, 37) that was up-regulated in retinal macrophages/microglia from OIR mice as compared to control mice (Fig. 1I and fig. S1F). Similar to $Pfkfb3^{\Delta M\phi}$, retinas *of* $Pkm2^{\Delta M\phi}$ mice exhibited a decrease in the number of

pathological neovascular tufts and in vascular permeability but an increase in physiological revascularization at P17, whereas no change in vaso-obliteration was observed at P12 (Fig. 3, D to F, and fig. S4, E to H). Collectively, these data indicate that inhibition of macrophage glycolysis suppresses pathological neovascularization in a mouse model of pathological retinal angiogenesis.

Soluble factors from RECs induce macrophage/microglia glycolysis and polarize macrophages/microglia toward a mixed M1/M2 phenotype

Our observations that macrophage/microglia glycolysis is critical for pathological retinal neovascularization and that these cells are found in close proximity to ECs prompted us to explore whether ECs play a role in switching these macrophages/microglia to glycolytic metabolism and proangiogenic behavior. We first incubated BMDMs with the conditioned medium (CM) of cultured RECs under normoxia or hypoxia (Nx-REC-CM or Hx-REC-CM, respectively), which mimic the in vivo microenvironments in RA or OIR retinas. Hx-REC-CM induced a marked increase in the mRNA expression of key glycolysis-related genes, especially *Pfkfb3*, in mouse BMDMs (Fig. 4A). Changes in the protein expression of Pfkfb3 paralleled changes in mRNA expression (Fig. 4, B and C). Similarly, the amount of intracellular glycolytic metabolite lactate was increased in Hx-REC-CM–treated BMDMs (Fig. 4D). Seahorse flux analysis also revealed that glycolysis was increased, whereas the mitochondrial respiratory activity was unchanged in BMDMs exposed to Hx-REC-CM (fig. S5, A to D). Isolated and cultured mouse retinal microglia also showed increased Pfkfb3 expression in response to Hx-REC-CM incubation (fig. S6A). Together, these results indicate that soluble factor(s) released from RECs, and especially hypoxic ECs, can induce glycolytic enzyme expression and glycolysis in adjacent macrophages/microglia.

We further characterized the activation profile and phenotypic changes in macrophages/microglia from the retinal angiogenic niche. Among $CD11b^+/F4/80^+$ macrophages/microglia isolated from mouse retinas, the percentage of $CD86^+$ (M1 marker) and $CD206^+$ (M2 marker) double-positive macrophages/microglia slightly fluctuated between 12 and ~25% from P12 to P25 in RA retinas. In contrast, the percentage of this population in OIR retinas escalated from ~10.6% at P12 to ~48.5% at P17 and then declined to ~29.8% at P25 (Fig. 4, E and F). These $CD86^+CD206^+$ macrophages/microglia also highly expressed other M1/M2 molecules such as CD80, CD163, Il1b, and Arg1 (fig. S7). The mRNA expression of these M1/M2 molecules paralleled with the dynamic of this M1/M2 macrophage/microglia population in the development of OIR (fig. S8). Immunofluorescence analysis of OIR retinas showed that most of the macrophages/microglia were CD11c and CD206 double-positive in neovascular tufts (fig. S9). Furthermore, the gene expression profile showed that the mRNA expression of many more M1/M2 markers, and proangiogenic factors were much higher in macrophages/microglia from OIR mice than those from RA controls (Fig. 4G). In contrast, the $CD11c^+CD206^+$ double-positive population of macrophages was not found in other tissues analyzed such as adipose tissue from mice fed a high-fat diet (HFD) (fig. S10). Together, these data indicate that macrophages/microglia in the retinal angiogenic niche exhibit a unique mixed M1/M2 phenotype. We termed these unique macrophages/microglia as PRAGMs.

A common characteristic of pathological angiogenesis with ischemic retinopathies is the formation of an oxygen-deficient microenvironment due to retinal nonperfusion (38). We therefore asked whether hypoxia alone is sufficient to induce the PRAGM phenotype. Whereas hypoxia up-regulated the mRNA expression of *Arg1*, *Retnla*, *Nos2*, and *Vegf* (fig. S11), it was not sufficient to cause an increase in the expression of other macrophage polarization markers or angiogenic genes observed in PRAGMs. Because PRAGMs are found in close proximity to hyperglycolytic ECs, we next tested whether ECs in the angiogenic vascular niche are responsible for macrophage/microglia polarization toward the unique proangiogenic phenotype. To this end, we incubated BMDMs with Nx-REC-CM and Hx-REC-CM. The CM polarized macrophages to cells with a phenotype resembling that of PRAGMs in the OIR retinas, as evidenced by increased cell surface markers of both M1 and M2 macrophages and both proinflammatory and proangiogenic factors (Fig. 4H). The Hx-REC-CM was more efficacious in driving these changes as compared with Nx-REC-CM (Fig. 4H). This phenotypic change also occurred in mouse retinal microglia after Hx-REC-CM treatment (fig. S6, B to G).

Reprogrammed glycolysis in macrophages/microglia supports its enhanced proangiogenic activity

Having shown that Hx-REC-CM promotes both macrophage glycolysis and activation, we next asked whether reprogrammed glycolysis in macrophages underlies their angiogenic activity. BMDMs from *Pfkfb3*$^{\Delta M\phi}$ mice had markedly decreased mRNA expression of *Pfkfb3*, a subset of M1 markers (especially *Il1b* and *Nos2*), M2 markers (especially *Arg1*, *Retnla*, and *Mgl2*), and proangiogenic genes (especially *Mmp2*, *Mmp9*, *Fgf2*, and *Hbegf*), compared with those of BMDMs from *Pfkfb3*^{WT} mice (fig. S12A). Similar results were obtained when BMDMs were exposed to Hx-REC-CM (Fig. 5A). Blocking glycolysis with 2-deoxyglucose also markedly inhibited Hx-REC-CM–induced gene expression in BMDMs (fig. S12B). IL-4, a well-characterized inducer for M2 polarization of macrophages/microglia, did not increase *Pfkfb3* expression or glycolytic function, and *Pkfkb3* deletion had no effects on IL-4–induced robust expression of M2 markers in BMDMs (fig. S13). To test whether similar changes also take place in PRAGMs in vivo, we isolated PRAGMs from *Pfkfb3*$^{\Delta M\phi}$ and control mice and assayed the cells with quantitative polymerase chain reaction (PCR). In line with the in vitro findings, PRAGM-associated genes were down-regulated in macrophages/microglia from OIR retinas of *Pfkfb3*$^{\Delta M\phi}$ mice compared with those from controls (Fig. 5B). Consistent with these observations, immunofluorescent staining showed decreased expression of proangiogenic cytokine Arg1 (Fig. 5, C and D), Il1b (Fig. 5, E and F), and Fgf2 (Fig. 5, G and H) in retinal macrophages/microglia of *Pfkfb3*$^{\Delta M\phi}$ mice with OIR. Furthermore, the flow cytometry results showed that the percentages of $CD11b^+F4/80^+CD206^+CD86^+$ cells were lower in P17 OIR retinas of *Pfkfb3*$^{\Delta M\phi}$ mice compared with those in OIR retinas of *Pfkfb3*^{WT} mice (Fig. 5, I and J). In contrast, the numbers of $CD11b^+F4/80^+$ macrophages/microglia and $CD11b^+$ $Ly6G^+$ neutrophils in both RA and OIR retinas of *Pfkfb3*^{WT} and *Pfkfb3*$^{\Delta M\phi}$ mice did not differ significantly ($P > 0.05$; fig. S14), suggesting a minor role of Pfkfb3 in leukocyte infiltration into retinas. These data indicate that reprogrammed endogenous glycolysis in macrophages/microglia is critical for macrophage/microglia activation.

Next, we evaluated the angiogenic effect of Pfkfb3-driven macrophage glycolysis on human RECs. As shown in Fig. 6 (A to C), CM *Pfkfb3*^{WT} BMDMs increased the proliferation of RECs, and CM of Hx-REC-CM–pretreated *Pfkfb3*^{WT} BMDMs promoted a greater increase in REC proliferation, as revealed by 5-bromo-2′-deoxyuridine (BrdU) incorporation and Ki-67 reactivity assays. However, the ability of CM from Hx-REC-CM–pretreated *Pfkfb3*$^{\Delta M\phi}$ BMDMs to enhance the proliferation of RECs was reduced compared to that of CM from Hx-REC-CM–pretreated *Pfkfb3*^{WT} BMDMs (Fig. 6, A to C). Similar results were obtained using two additional models of in vitro angiogenesis in which human RECs form a two-dimensional vessel network and three-dimensional spheroids (Fig. 6, D to I). We also analyzed the potential effects of *Pfkfb3* deficiency on macrophage survival and proliferation, which could influence the secretion of angiogenic factors by macrophages and the angiogenic readouts. We noted no difference in macrophage proliferation and viability between genotypes, as evidenced by BrdU incorporation and WST-1 assays (fig. S15).

The effect of macrophage glycolysis on EC proliferation and sprouting were further evaluated using ex vivo angiogenesis models. CM from Hx-REC-CM–pretreated BMDMs increased the sprouting of both aortic rings and choroidal explants as compared with CM from BMDMs not pretreated with Hx-REC-CM, and these proangiogenic effects were reduced when using CM from BMDMs treated with small interfering RNA of Mmp9 and Il1β or their neutralizing antibodies or from *Pfkfb3*-deficient BMDMs (Fig. 6, J to M, and fig. S16). These results suggest that Pfkfb3-driven glycolysis in macrophages promotes sprouting and angiogenesis through changes in macrophage activation and increased secretion of proinflammatory and proangiogenic factors.

To demonstrate the ability of macrophages and vascular ECs to reciprocally activate each other, the effects of BMDM-CM and cocultures with ECs and BMDMs on angiogenesis in the ex vivo aortic explant model in Transwells were compared (Fig. 6N). Coculture with BMDMs induced greater vessel sprouting than BMDM-CM (Fig. 6, N and O), suggesting that the proangiogenic activity of macrophages is stimulated by the presence of vascular ECs in the cocultures. Furthermore, an increase in Pfkfb3 expression was observed in vascular ECs cocultured with BMDMs compared to ECs exposed to control medium or BMDM-CM (Fig. 6P). These data indicate that reciprocal interactions between macrophages and ECs result in mutual activations.

Lactate from RECs is sufficient to induce macrophage/microglia glycolysis and phenotypic change

Having shown that Hx-REC-CM induces macrophage activation via reprogramming toward enhanced glycolysis, we next sought to identify the soluble factor(s) in REC-CM that are capable of promoting macrophage glycolysis. We fractionated REC-CM by size (<3 and >3 kDa) using 3K centrifugal filters and tested the activity of both fractions. Both unfractionated CM and the <3-kDa fraction markedly increased the *Pfkfb3* mRNA expression by ~8-fold (Fig. 7A), whereas the >3-kDa fraction did not show this effect. Furthermore, the <3-kDa fraction robustly up-regulated the expression of macrophage polarization markers and proangiogenic factors (fig. S17, A to F). In addition, the boiling of Hx-REC-CM did not impair its ability to strongly up-regulate *Pfkfb3* expression (fig. S17G).

These results indicate that the active soluble factor(s) in the REC-CM are heat stable and likely to be metabolite (s) with low molecular weight (<3 kDa).

Lactate and pyruvate are the major metabolites of glycolysis released by cultured ECs (39) and hypoxic diabetic retinas (40). We therefore next tested whether REC-derived pyruvate or lactate can replicate the actions of the soluble factor(s) responsible for macrophage activation. ECs prefer aerobic glycolysis and convert most of their glucose to lactate regardless of the availability of sufficient oxygen in the blood (5). Hypoxia up-regulated the expression of Pfkfb3 and promoted the secretion of lactate in RECs (fig. S17, H to J). The lactate concentration was approximately 9.8 mM in Hx-REC-CM and ~5.7 mM in Nx-REC-CM and ~0.3 mM in control medium under the conditions used (Fig. 7B). In contrast, the concentration of pyruvate was much lower than that of lactate in Hx-REC-CM (0.16 ± 0.004 mM versus 9.76 ± 0.223 mM, $n = 6$) (fig. S17K).

As a small molecule, the vast majority of the lactate in Hx-REC-CM partitioned into the <3-kDa fraction, and lactate alone was sufficient to induce the expression of glycolytic genes, particularly *Pfkfb3* (Fig. 7C). In addition, lactate up-regulated the mRNA expression of PRAGM-related genes in BMDMs in a dose-dependent manner over a range of 3 to 20 mM (Fig. 7D), which are concentrations similar to the range observed in REC-CM, and correlate fairly well with gene induction by Hx-REC-CM (Fig. 4, A and H). Similarly, Pfkfb3 expression at the protein level paralleled changes in mRNA level (Fig. 7, E and F). Furthermore, Hx-REC-CM–induced up-regulation of *Pfkfb3* and proangiogenic genes was almost completely reversed by α-cyano-4-hydroxycinnamic acid (α-CHA), an inhibitor of monocarboxylate transporters (MCTs) (Fig. 7G), suggesting that cellular uptake of lactate by MCTs is necessary for the Hx-REC-CM–mediated macrophage activation. CM from human RECs in which *PFKFB3* was silenced had a low amount of lactate production (fig. S17, L and M), and incubation of CM from these cells with BMDMs resulted in lower mRNA expression of *Pfkfb3* and PRAGM-related genes (fig. S17N). The genetic phenotype of BMDMs treated with Hx-REC-CM was not due to pH alteration because pHs ranging from 7.55 to 6.35 did not significantly change the expression of these genes ($P > 0.05$; fig. S18). These results were corroborated in an in vivo study in the OIR model, in which EC-specific deletion of *Pfkfb3* attenuated lactate production (Fig. 7H), the expression of *Pfkfb3* and markers of the M1/M2 phenotype in retinal macrophages/microglia (Fig. 7I), suppressed macrophage/microglia polarization toward the PRAGM phenotype (Fig. 7, J and K) and ultimately led to a reduction in neovascular tuft area in OIR retinas (Fig. 7, L to N). In particular, the pathological neovascularization was markedly reduced in myeloid cells and EC *Pfkfb3* double-KO pups as compared to WT groups and myeloid cell or EC *Pfkfb3* single-KO mice (Fig. 7, L to N). These data are congruent with the concept that Pfkfb3-mediated glycolysis is critical for the reciprocal activation between macrophages/microglia and ECs in the retinal angiogenic niche.

Histone acetylation mediates metabolic reprograming and angiogenic activities of PRAGMs.

Metabolic status has been previously linked to macrophage activation (19), but the mechanisms underlying changes in the specific gene expression profile of PRAGMs

mediated by glycolysis remain poorly characterized. We therefore explored whether glycolysis-mediated production of Ac-CoA and subsequent histone acetylation underlie glycolysis-mediated gene induction during macrophage activation. Hx-REC-CM treatment led to a ~35% increase in the amount of Ac-CoA in BMDMs (Fig. 8A). Blocking macrophage glycolysis by the silencing of *Pfkfb3* suppressed both basal and Hx-REC-CM–mediated Ac-CoA production (Fig. 8A). Ac-CoA is a substrate of acetylation, and we postulated that an increase in the amount of Ac-CoA might affect histone acetylation in macrophages. To test this hypothesis, we stained macrophages with antibodies for Ac-H3 and Ac-H4, two well-known pan-acetylation markers, after incubation with control medium or Hx-REC-CM. Hx-REC-CM incubation enhanced acetylation of H3 and H4 histones of macrophages, and the expression of Ac-H3 and Ac-H4 was reduced in *Pfkfb3*$^{\Delta M\phi}$ macrophages (Fig. 8, B to E), indicating that histone acetylation in these macrophages is at least partially dependent on glycolysis. Similar results were obtained by Western blot (Fig. 8, F to H). Anacardic acid (ANAC), a histone acetyltransferase inhibitor, or BMS 303141, a specific inhibitor of adenosine 5′-triphosphate citrate lyase (ACLY), which is a major enzyme responsible for Ac-CoA production for histone acetylation (Fig. 8I), potently inhibited the Hx-REC-CM–induced expression of macrophage polarization markers and proangiogenic factors (fig. S19), as well as the angiogenic effects, as indicated by analysis of sprouting of choroidal explants (Fig. 8, J and K). Last, we investigated gene-specific patterns of H3 and H4 acetylation by chromatin immunoprecipitation (ChIP) analysis. As shown in Fig. 8, L to O, both Ac-H3 and Ac-H4 on the promoters of M1/M2 and proangiogenic genes were high. ChIP assay results further showed that Hx-REC-CM markedly increased the amount of acetylation of H3 and H4 histones at the promoters of these genes (Fig. 8, L to O). *Pfkfb3* deletion attenuated REC-CM–mediated recruitment of acetylated H3 and H4 to the promoters of most of the genes examined except the housekeeping gene *Rpl13a* (Fig. 8, L to O). Overall, these findings suggest that glycolysis-regulated production of Ac-CoA drives histone acetylation, which is the predominant mechanism underlying the induction of PRAGM-associated genes.

DISCUSSION

Here, we have uncovered a glycolysis-dependent paracrine relationship between RECs and neighboring macrophages/microglia in the setting of pathological retinal angiogenesis. RECs secrete glycolytic metabolites, in particular lactate, that trigger changes in local macrophage/microglia metabolism to favor a hyperglycolytic state. These PRAGMs have a unique angiogenic phenotype that includes increased expression of both M1 and M2 markers and enhanced production of both proinflammatory and proangiogenic cytokines. These factors reciprocally enhance REC glycolysis, resulting in EC sprouting and proliferation and ultimately pathological neovascularization. Suppression of glycolysis by knockdown of *Pfkfb3* in either macrophages/microglia or ECs impairs the polarization of macrophages/microglia toward proangiogenic phenotypes and alleviates pathological retinal angiogenesis in mice. At molecular level, PRAGMs produce large amount of Ac-CoA, leading to epigenetic reprogramming via histone acetylation that favors the up-regulation of PRAGM-associated genes encoding a macrophage-angiogenic phenotype (fig. S20).

A salient observation in this study is that PRAGMs exhibit a unique mixed M1/M2-like phenotype. Previous studies have characterized the most prominent macrophage population in retinal angiogenesis as M2 macrophages (16, 17), whereas recent studies using ischemic mouse retinas or injured choroids (laser-induced choroidal neovascularization model) have demonstrated the up-regulation of macrophage surface markers for both the M1 and M2 subtypes (17, 41). These studies have suggested the coexistence of M1 and M2 macrophages, two separate populations of macrophages, in mouse hypoxic retinas. In contrast, using quantitative reverse transcription PCR (qRT-PCR), immunofluorescence, and flow cytometry, we consistently found that most macrophages/microglia in the setting of pathological retinal neovascularization coexpress markers of both the M1 and M2 subtypes. In addition, these macrophages/microglia produce both proinflammatory and proangiogenic cytokines. These data not only reflect the high plasticity of macrophages/microglia but also suggest that a unique microenvironment in the niche of pathological angiogenesis is able to polarize macrophages/microglia to a hybrid state. This is consistent with a recent study showing that the CM of pancreatic ductal adenocarcinoma cells induces macrophages to express cell surface markers of both M1 and M2 macrophages and produce both proinflammatory and proangiogenic cytokines (42). Glycolytic metabolites largely induce a unique hybrid M1/M2 phenotype. However, considering the heterogeneity of macrophages, it cannot be excluded that these metabolites may still be able to differentiate small populations of macrophages to separate M1 or M2 phenotypes.

Endogenous macrophage glycolysis is required for the induction of the unique phenotype of PRAGMs. A previous study has shown that lactate induces an M2-like phenotype via stabilization of hypoxia-inducible factor-1α (HIF-1α) (14), suggesting that lactate can preserve the protein expression of HIF-1α in macrophages, which increases HIF-1 transcriptional activity to enhance expression of M2 cytokines. In contrast, in the current study, lactate induced a unique hybrid M1/M2 phenotype in macrophages, which expands on the existing knowledge of macrophage/microglia subtypes in retinal angiogenesis. The number of PRAGMs was markedly decreased in OIR retinas of *Pfkfb3*$^{\Delta M\phi}$ mice compared to WT, and the expression of macrophage polarization markers and cytokines released by PRAGMs was decreased in *Pfkfb3* KO macrophages/microglia incubated with Hx-REC-CM. These observations suggest that Pfkfb3-dependent glycolysis is required for the full induction of the PRAGM phenotype in response to exogenous glycolytic metabolites. It is conceivable that exogenous glycolytic metabolites may initially raise glycolysis or glucose metabolism in macrophages by up-regulating glycolytic enzymes and regulators, and then, subsequent metabolites from endogenous glycolysis or glucose metabolism, particularly pyruvate and Ac-CoA, signal to induce the unique phenotype of PRAGMs.

The reciprocal interaction between macrophages and ECs promotes a feed-forward relationship that strongly augments angiogenesis. In this study, *Pfkfb3* knockdown inhibits the release of proinflammatory and proangiogenic factors from macrophages and the production of lactate by RECs, thus blocking this positive feedback loop. Congruently, in an OIR mouse model, pathological neovascularization was markedly decreased in macrophage and EC *Pfkfb3* double-KO pups as compared to those of WT, macrophage, or EC *Pfkfb3* single-KO pups, suggesting that targeting the reciprocal activation of macrophage and EC glycolysis may be an efficient therapeutic strategy for treating pathologic retinal

angiogenesis. To this end, approaches including inhibiting the activity of PFKFB3 or pyruvate kinase isoenzyme type M2 (PKM2), or blocking lactate uptake with inhibitors of MCTs, may hold promise if their suitability as therapeutic targets are demonstrated in preclinical models. Furthermore, given that macrophage glycolysis is required for homeostasis of the innate immune system (33), local administration of these inhibitors via intravitreal injections should be able to effectively block these reciprocal metabolic interactions between macrophages/microglia and RECs without inhibiting the systemic innate immune system.

Our study has some limitations. We used *Lysm*-Cre transgenic mice to generate mice deficient in *Pfkfb3* in myeloid cells. Use of these mice did not allow us to distinguish the extent of the individual contributions from microglia or macrophage Pfkfb3 to retinal angiogenesis, although that *Pfkfb3* deficiency exhibited a similar effect on both types of cells. Besides, we focus on the effect of Pfkfb3 in macrophages and microglia in the retinal phenotype in this study because these cells, either resident in retinas or differentiated from bone marrow–derived monocytes (43, 44), have been demonstrated to be major players in pathological retinal angiogenesis (9, 11); however, the role of Pfkfb3 deficiency in other myeloid cells, including neutrophils, in regulation of the retinal phenotype cannot be excluded and warrants further investigation. Furthermore, the current studies focused on the effect of Pfkfb3 deficiency on retinal angiogenesis. Nevertheless, considering the translational nature of this study, effects of this pathway on the functions and viability of retinal neuron cells should be also studied in the future. A recent study reported that suppression of PKM2, another key glycolytic enzyme, compromised function of photoreceptor cells (45). This indicates that to select a safe target among glycolytic enzymes/regulators, a comprehensive study of functional influence of each glycolytic enzyme on the entire ocular system is warranted. Last, in future research, the effect of EC–myeloid cell metabolic interactions on other types of ocular angiogenesis such as AMD as well as ocular angiogenesis models in other types of animals should also be considered.

MATERIALS AND METHODS

Study design

The major goal of this study was to define the effect of metabolic interactions between RECs and myeloid cells on the development of pathological retinal angiogenesis in vitro and in vivo. In vivo experiments for loss-of-function studies were performed in a model of OIR with mice deficient in Pfkfb3 in ECs, myeloid cells, or both. In addition, RECs or myeloid cells from these mice were isolated, and their angiogenetic activities were evaluated with molecular and cellular approaches. Experimental groups were composed of at least six mice per group to robustly demonstrate the difference in angiogenic phenotypes or/and expression of the relevant genes. Mice were randomly assigned to the control and OIR groups. Mouse pups were weighed, and underdeveloped neonatal mice with very low body weight were excluded. Data analyses for in vivo angiogenic phenotype were performed in a blinded fashion. The control and treatment groups, the sample sizes, and the individual statistical test used for each experiment are specified in the figure legends. All the original data are in data file S1.

Statistical analysis

Data are presented as means ± SEM, unless otherwise specified. Statistical analysis was performed using GraphPad Prism Software (La Jolla, CA). After the normal distribution was confirmed with the Kolmogorov-Smirnov test, statistical comparisons were done using two-tailed unpaired Student's *t* test or one- or two-way analysis of variance (ANOVA) followed by Bonferroni's post hoc tests when appropriate. Two-sided *P* values were calculated, and $P < 0.05$ denoted significance. Statistical significance was defined as follows: $*P < 0.05$, $**P < 0.01$, and $***P < 0.001$. ns, not significant.

Supplementary Material

Refer to Web version on PubMed Central for supplementary material.

Acknowledgments

Funding: This work was supported by grants from the National Natural Science Foundation of China (81870324 to Z.L.), the Shenzhen Science and Technology Innovation Committee (JCYJ20190808155605447 and JCYJ20170810163238384 to Z.L.; JCYJ20170412150405310, JCYJ20190808155801648, and 2019SHIBS0004 to M.H.), the American Heart Association (19POST34430119 to Z.L. and 19TPA34910043 to Y.H.), and the National Institutes of Health (R01 EY030500 and R01 HL134934 to Y.H., R01 HL142097 to N.L.W., IK6 RX005228 and EY011766 to R.B.C., R01 EY017017 and EY030904 to L.E.H.S., R01 EY030140 and EY029238 to Y.S., R01HL147159 to D.J.F., and R01 EY029750 to A.T.). Z.D. is a recipient of VA Senior Research Career award.

REFERENCES AND NOTES

1. Penn JS, Madan A, Caldwell RB, Bartoli M, Caldwell RW, Hartnett ME, Vascular endothelial growth factor in eye disease. Prog. Retin. Eye Res 27, 331–371 (2008). [PubMed: 18653375]
2. Chen J, Stahl A, Krah NM, Seaward MR, Dennison RJ, Sapieha P, Hua J, Hatton CJ, Juan AM, Aderman CM, Willett KL, Guerin KI, Mammoto A, Campbell M, Smith LE, Wnt signaling mediates pathological vascular growth in proliferative retinopathy. Circulation 124, 1871–1881 (2011). [PubMed: 21969016]
3. Rama N, Dubrac A, Mathivet T, Ni Charthaigh RA, Genet G, Cristofaro B, Pibouin-Fragner L, Ma L, Eichmann A, Chedotal A, Slit2 signaling through Robo1 and Robo2 is required for retinal neovascularization. Nat. Med 21, 483–491 (2015). [PubMed: 25894826]
4. Carmeliet P, De Smet F, Loges S, Mazzone M, Branching morphogenesis and antiangiogenesis candidates: Tip cells lead the way. Nat. Rev. Clin. Oncol 6, 315–326 (2009). [PubMed: 19483738]
5. De Bock K, Georgiadou M, Schoors S, Kuchnio A, Wong BW, Cantelmo AR, Quaegebeur A, Ghesquiere B, Cauwenberghs S, Eelen G, Phng LK, Betz I, Tembuyser B, Brepoels K, Welti J, Geudens I, Segura I, Cruys B, Bifari F, Decimo I, Blanco R, Wyns S, Vangindertael J, Rocha S, Collins RT, Munck S, Daelemans D, Imamura H, Devlieger R, Rider M, Van Veldhoven PP, Schuit F, Bartrons R, Hofkens J, Fraisl P, Telang S, Deberardinis RJ, Schoonjans L, Vinckier S, Chesney J, Gerhardt H, Dewerchin M, Carmeliet P, Role of PFKFB3-driven glycolysis in vessel sprouting. Cell 154, 651–663 (2013). [PubMed: 23911327]
6. Xu Y, An X, Guo X, Habtetsion TG, Wang Y, Xu X, Kandala S, Li Q, Li H, Zhang C, Caldwell RB, Fulton DJ, Su Y, Hoda MN, Zhou G, Wu C, Huo Y, Endothelial PFKFB3 plays a critical role in angiogenesis. Arterioscler. Thromb. Vasc. Biol 34, 1231–1239 (2014). [PubMed: 24700124]
7. Schoors S, De Bock K, Cantelmo AR, Georgiadou M, Ghesquiere B, Cauwenberghs S, Kuchnio A, Wong BW, Quaegebeur A, Goveia J, Bifari F, Wang X, Blanco R, Tembuyser B, Cornelissen I, Bouche A, Vinckier S, Diaz-Moralli S, Gerhardt H, Telang S, Cascante M, Chesney J, Dewerchin M, Carmeliet P, Partial and transient reduction of glycolysis by PFKFB3 blockade reduces pathological angiogenesis. Cell Metab. 19, 37–48 (2014). [PubMed: 24332967]

8. Kataoka K, Nishiguchi KM, Kaneko H, van Rooijen N, Kachi S, Terasaki H, The roles of vitreal macrophages and circulating leukocytes in retinal neovascularization. Invest. Ophthalmol. Vis. Sci 52, 1431–1438 (2011). [PubMed: 21051720]
9. Kubota Y, Takubo K, Shimizu T, Ohno H, Kishi K, Shibuya M, Saya H, Suda T, M-CSF inhibition selectively targets pathological angiogenesis and lymphangiogenesis. J. Exp. Med 206, 1089–1102 (2009). [PubMed: 19398755]
10. Fantin A, Vieira JM, Gestri G, Denti L, Schwarz Q, Prykhozhij S, Peri F, Wilson SW, Ruhrberg C, Tissue macrophages act as cellular chaperones for vascular anastomosis downstream of VEGF-mediated endothelial tip cell induction. Blood 116, 829–840 (2010). [PubMed: 20404134]
11. Dejda A, Mawambo G, Cerani A, Miloudi K, Shao Z, Daudelin JF, Boulet S, Oubaha M, Beaudoin F, Akla N, Henriques S, Menard C, Stahl A, Delisle JS, Rezende FA, Labrecque N, Sapieha P, Neuropilin-1 mediates myeloid cell chemoattraction and influences retinal neuroimmune crosstalk. J. Clin. Invest 124, 4807–4822 (2014). [PubMed: 25271625]
12. Mosser DM, Edwards JP, Exploring the full spectrum of macrophage activation. Nat. Rev. Immunol 8, 958–969 (2008). [PubMed: 19029990]
13. Sica A, Mantovani A, Macrophage plasticity and polarization: In vivo veritas. J. Clin. Invest 122, 787–795 (2012). [PubMed: 22378047]
14. Colegio OR, Chu NQ, Szabo AL, Chu T, Rhebergen AM, Jairam V, Cyrus N, Brokowski CE, Eisenbarth SC, Phillips GM, Cline GW, Phillips AJ, Medzhitov R, Functional polarization of tumour-associated macrophages by tumour-derived lactic acid. Nature 513, 559–563 (2014). [PubMed: 25043024]
15. Wang Q, He Z, Huang M, Liu T, Wang Y, Xu H, Duan H, Ma P, Zhang L, Zamvil SS, Hidalgo J, Zhang Z, O'Rourke DM, Dahmane N, Brem S, Mou Y, Gong Y, Fan Y, Vascular niche IL-6 induces alternative macrophage activation in glioblastoma through HIF-2α. Nat. Commun 9, 559 (2018). [PubMed: 29422647]
16. Zhou Y, Yoshida S, Nakao S, Yoshimura T, Kobayashi Y, Nakama T, Kubo Y, Miyawaki K, Yamaguchi M, Ishikawa K, Oshima Y, Akashi K, Ishibashi T, M2 macrophages enhance pathological neovascularization in the mouse model of oxygen-induced retinopathy. Invest. Ophthalmol. Vis. Sci 56, 4767–4777 (2015). [PubMed: 26218904]
17. Yang Y, Liu F, Tang M, Yuan M, Hu A, Zhan Z, Li Z, Li J, Ding X, Lu L, Macrophage polarization in experimental and clinical choroidal neovascularization. Sci. Rep 6, 30933 (2016). [PubMed: 27489096]
18. Sun Y, Liu CH, SanGiovanni JP, Evans LP, Tian KT, Zhang B, Stahl A, Pu WT, Kamenecka TM, Solt LA, Chen J, Nuclear receptor RORα regulates pathologic retinal angiogenesis by modulating SOCS3-dependent inflammation. Proc. Natl. Acad. Sci. U.S.A 112, 10401–10406 (2015). [PubMed: 26243880]
19. Langston PK, Shibata M, Horng T, Metabolism supports macrophage activation. Front. Immunol 8, 61 (2017). [PubMed: 28197151]
20. Huang SC, Smith AM, Everts B, Colonna M, Pearce EL, Schilling JD, Pearce EJ, Metabolic reprogramming mediated by the mTORC2-IRF4 signaling axis is essential for macrophage alternative activation. Immunity 45, 817–830 (2016). [PubMed: 27760338]
21. Biswas SK, Mantovani A, Orchestration of metabolism by macrophages. Cell Metab. 15, 432–437 (2012). [PubMed: 22482726]
22. Galvan-Pena S, O'Neill LA, Metabolic reprograming in macrophage polarization. Front. Immunol 5, 420 (2014). [PubMed: 25228902]
23. Moussaieff A, Rouleau M, Kitsberg D, Cohen M, Levy G, Barasch D, Nemirovski A, Shen-Orr S, Laevsky I, Amit M, Bomze D, Elena-Herrmann B, Scherf T, Nissim-Rafinia M, Kempa S, Itskovitz-Eldor J, Meshorer E, Aberdam D, Nahmias Y, Glycolysis-mediated changes in acetyl-CoA and histone acetylation control the early differentiation of embryonic stem cells. Cell Metab. 21, 392–402 (2015). [PubMed: 25738455]
24. Shyh-Chang N, Daley GQ, Metabolic switches linked to pluripotency and embryonic stem cell differentiation. Cell Metab. 21, 349–350 (2015). [PubMed: 25738450]

25. Wellen KE, Hatzivassiliou G, Sachdeva UM, Bui TV, Cross JR, Thompson CB, ATP-citrate lyase links cellular metabolism to histone acetylation. Science 324, 1076–1080 (2009). [PubMed: 19461003]
26. Rathmell JC, Newgard CB, Biochemistry. A glucose-to-gene link. Science 324, 1021–1022 (2009). [PubMed: 19460991]
27. Covarrubias AJ, Aksoylar HI, Yu J, Snyder NW, Worth AJ, Iyer SS, Wang J, Ben-Sahra I, Byles V, Polynne-Stapornkul T, Espinosa EC, Lamming D, Manning BD, Zhang Y, Blair IA, Horng T, Akt-mTORC1 signaling regulates Acly to integrate metabolic input to control of macrophage activation. eLife 5, e11612 (2016). [PubMed: 26894960]
28. Smith LE, Wesolowski E, McLellan A, Kostyk SK, D'Amato R, Sullivan R, D'Amore PA, Oxygen-induced retinopathy in the mouse. Invest. Ophthalmol. Vis. Sci 35, 101–111 (1994). [PubMed: 7507904]
29. Outtz HH, Tattersall IW, Kofler NM, Steinbach N, Kitajewski J, Notch1 controls macrophage recruitment and Notch signaling is activated at sites of endothelial cell anastomosis during retinal angiogenesis in mice. Blood 118, 3436–3439 (2011). [PubMed: 21795743]
30. Birdsey GM, Shah AV, Dufton N, Reynolds LE, Osuna Almagro L, Yang Y, Aspalter IM, Khan ST, Mason JC, Dejana E, Gottgens B, Hodivala-Dilke K, Gerhardt H, Adams RH, Randi AM, The endothelial transcription factor ERG promotes vascular stability and growth through Wnt/β-Catenin signaling. Dev. Cell 32, 82–96 (2015). [PubMed: 25584796]
31. Liu Z, Yan S, Wang J, Xu Y, Wang Y, Zhang S, Xu X, Yang Q, Zeng X, Zhou Y, Gu X, Lu S, Fu Z, Fulton DJ, Weintraub NL, Caldwell RB, Zhang W, Wu C, Liu XL, Chen JF, Ahmad A, Kaddour-Djebbar I, Al-Shabrawey M, Li Q, Jiang X, Sun Y, Sodhi A, Smith L, Hong M, Huo Y, Endothelial adenosine A2a receptor-mediated glycolysis is essential for pathological retinal angiogenesis. Nat. Commun 8, 584 (2017). [PubMed: 28928465]
32. Kelly B, O'Neill LA, Metabolic reprogramming in macrophages and dendritic cells in innate immunity. Cell Res. 25, 771–784 (2015). [PubMed: 26045163]
33. Jiang H, Shi H, Sun M, Wang Y, Meng Q, Guo P, Cao Y, Chen J, Gao X, Li E, Liu J, PFKFB3-driven macrophage glycolytic metabolism is a crucial component of innate antiviral defense. J. Immunol 197, 2880–2890 (2016). [PubMed: 27566823]
34. Palsson-McDermott EM, Curtis AM, Goel G, Lauterbach MA, Sheedy FJ, Gleeson LE, van den Bosch MW, Quinn SR, Domingo-Fernandez R, Johnston DG, Jiang JK, Israelsen WJ, Keane J, Thomas C, Clish C, Vander Heiden M, Xavier RJ, O'Neill LA, Pyruvate kinase M2 regulates Hif-1α activity and IL-1β induction and is a critical determinant of the warburg effect in LPS-activated macrophages. Cell Metab. 21, 65–80 (2015). [PubMed: 25565206]
35. Van Schaftingen E, Lederer B, Bartrons R, Hers HG, A kinetic study of pyrophosphate: fructose-6-phosphate phosphotransferase from potato tubers. Application to a microassay of fructose 2,6-bisphosphate. Eur. J. Biochem 129, 191–195 (1982). [PubMed: 6297885]
36. Li FL, Liu JP, Bao RX, Yan G, Feng X, Xu YP, Sun YP, Yan W, Ling ZQ, Xiong Y, Guan KL, Yuan HX, Acetylation accumulates PFKFB3 in cytoplasm to promote glycolysis and protects cells from cisplatin-induced apoptosis. Nat. Commun 9, 508 (2018). [PubMed: 29410405]
37. Xie M, Yu Y, Kang R, Zhu S, Yang L, Zeng L, Sun X, Yang M, Billiar TR, Wang H, Cao L, Jiang J, Tang D, PKM2-dependent glycolysis promotes NLRP3 and AIM2 inflammasome activation. Nat. Commun 7, 13280 (2016). [PubMed: 27779186]
38. Keshet E, More weapons in the arsenal against ischemic retinopathy. J. Clin. Invest 107, 945–946 (2001). [PubMed: 11306596]
39. Eelen G, de Zeeuw P, Treps L, Harjes U, Wong BW, Carmeliet P, Endothelial cell metabolism. Physiol. Rev 98, 3–58 (2018). [PubMed: 29167330]
40. Barba I, Garcia-Ramirez M, Hernandez C, Alonso MA, Masmiquel L, Garcia-Dorado D, Simo R, Metabolic fingerprints of proliferative diabetic retinopathy: An 1H-NMR–Based metabonomic approach using vitreous humor. Invest. Ophthalmol. Vis. Sci 51, 4416–4421 (2010). [PubMed: 20375324]
41. Gao S, Li C, Zhu Y, Wang Y, Sui A, Zhong Y, Xie B, Shen X, PEDF mediates pathological neovascularization by regulating macrophage recruitment and polarization in the mouse model of oxygen-induced retinopathy. Sci. Rep 7, 42846 (2017). [PubMed: 28211523]

42. Penny HL, Sieow JL, Adriani G, Yeap WH, See Chi Ee P, San Luis B, Lee B, Lee T, Mak SY, Ho YS, Lam KP, Ong CK, Huang RY, Ginhoux F, Rotzschke O, Kamm RD, Wong SC, Warburg metabolism in tumor-conditioned macrophages promotes metastasis in human pancreatic ductal adenocarcinoma. Oncoimmunology 5, e1191731 (2016). [PubMed: 27622062]
43. Kohno H, Koso H, Okano K, Sundermeier TR, Saito S, Watanabe S, Tsuneoka H, Sakai T, Expression pattern of Ccr2 and Cx3cr1 in inherited retinal degeneration. J. Neuroinflammation 12, 188 (2015). [PubMed: 26458944]
44. O'Koren EG, Mathew R, Saban DR, Fate mapping reveals that microglia and recruited monocyte-derived macrophages are definitively distinguishable by phenotype in the retina. Sci. Rep 6, 20636 (2016). [PubMed: 26856416]
45. Petit L, Ma S, Cipi J, Cheng SY, Zieger M, Hay N, Punzo C, Aerobic glycolysis is essential for normal rod function and controls secondary cone death in retinitis pigmentosa. Cell Rep. 23, 2629–2642 (2018). [PubMed: 29847794]
46. Connor KM, Krah NM, Dennison RJ, Aderman CM, Chen J, Guerin KI, Sapieha P, Stahl A, Willett KL, Smith LE, Quantification of oxygen-induced retinopathy in the mouse: A model of vessel loss, vessel regrowth and pathological angiogenesis. Nat. Protoc 4, 1565–1573 (2009). [PubMed: 19816419]
47. Joyal JS, Sun Y, Gantner ML, Shao Z, Evans LP, Saba N, Fredrick T, Burnim S, Kim JS, Patel G, Juan AM, Hurst CG, Hatton CJ, Cui Z, Pierce KA, Bherer P, Aguilar E, Powner MB, Vevis K, Boisvert M, Fu Z, Levy E, Fruttiger M, Packard A, Rezende FA, Maranda B, Sapieha P, Chen J, Friedlander M, Clish CB, Smith LE, Retinal lipid and glucose metabolism dictates angiogenesis through the lipid sensor Ffar1. Nat. Med 22, 439–445 (2016). [PubMed: 26974308]
48. Roque RS, Caldwell RB, Isolation and culture of retinal microglia. Curr. Eye Res 12, 285–290 (1993). [PubMed: 7683260]
49. Zhang M, Zeng X, Yang Q, Xu J, Liu Z, Zhou Y, Cao Y, Zhang X, An X, Xu Y, Huang L, Han Z, Wang T, Wu C, Fulton DJ, Weintraub NL, Hong M, Huo Y, Ablation of Myeloid ADK (Adenosine Kinase) Epigenetically Suppresses Atherosclerosis in ApoE$^{-/-}$ (Apolipoprotein E Deficient) Mice. Arterioscler. Thromb. Vasc. Biol 38, 2780–2792 (2018). [PubMed: 30571174]

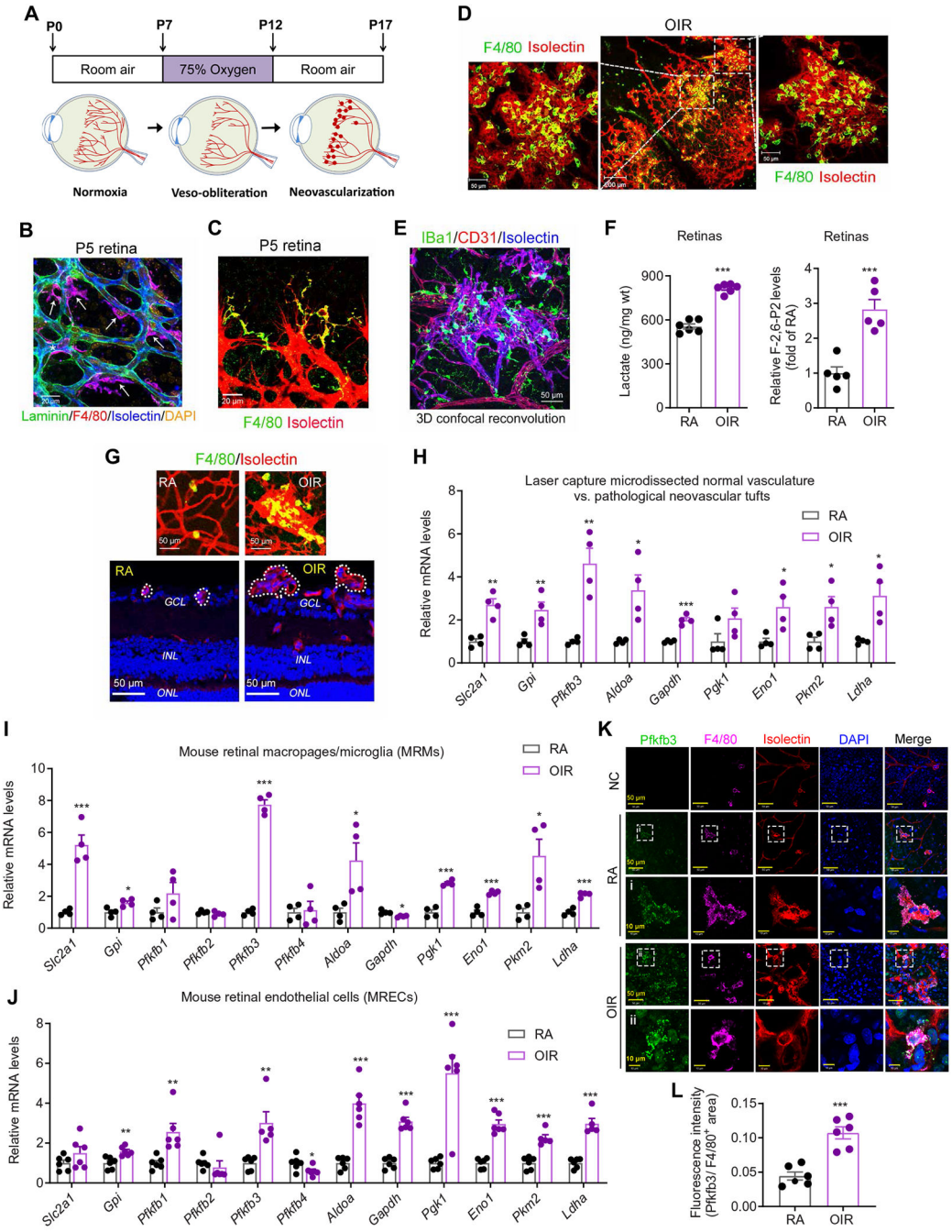

Fig. 1. Retinal macrophages/microglia are associated with ECs and are highly glycolytic in a pathological angiogenic niche.

(**A**) Schematic illustration of mouse OIR model. Neonatal mice with nursing mothers were exposed to 75% O_2 from postnatal day 7 (P7) to P12, followed by room air (RA) with maximum neovascularization (NV) at P17. (**B**) Triple immunohistochemistry (IHC) staining of laminin, F4/80, and isolectin B4 within the retina at P5. Scale bar, 20 μm. DAPI, 4′,6-diamidino-2-phenylindole. (**C**) Double IHC staining of F4/80 and isolectin B4 within the P5 retina. Scale bar, 20 μm. (**D**) Double immunofluorescent staining of F4/80 and isolectin B4

in retinas of OIR at P17. Scale bars, 50 or 100 μm. $n = 4$. (**E**) Triple IHC staining of IBa1, CD31, and isolectin B4 within the OIR retina at P17. Representative images are shown ($n =$ 6 retinas/mice). 3D, three-dimensional. (**F**) The amount of lactate ($n = 6$) or fructose 2,6-bisphosphate (F-2,6-P2) ($n = 5$) in RA or OIR retinas at P17. (**G**) Laser capture microdissection of macrophage/microglia-rich pathological tufts: double IHC staining of F4/80 and isolectin B4 on the frozen section of RA and OIR retina at P17. Dashed circles depict the dissection area by laser capture. GCL, ganglion cell layer; INL, inner nuclear layer; ONL, outer nuclear layer. Scale bars, 50 μm. (**H**) qRT-PCR analysis of the mRNA expression of glycolytic genes in retinal blood vessels isolated with laser capture microdissection from RA and OIR mice at P17 ($n = 4$). (**I** and **J**) qRT-PCR analysis of the mRNA expression of glycolytic genes in mouse retinal macrophages/microglia (MRMs, $n =$ 4) (I) or ECs (MRECs, $n = 5$ to 6) (J) isolated from RA and OIR mice at P17. (**K** and **L**) Pfkfb3 immunofluorescent staining of retinas from RA and OIR mice at P17. Representative Pfkfb3 (green), F4/80 (pink), isolectin B4 (red), DAPI (nuclei, blue), and merged images captured with confocal fluorescent microscopy (K). $n = 6$ mice for each group. NC, negative control (without Pfkfb3 primary antibody). The fluorescence intensity of Pfkfb3 staining was calculated by ImageJ software (L). Data are means ± SEM. $^{*}P < 0.05$; $^{**}P < 0.01$; $^{***}P < 0.001$ versus control group, by Student's *t* test.

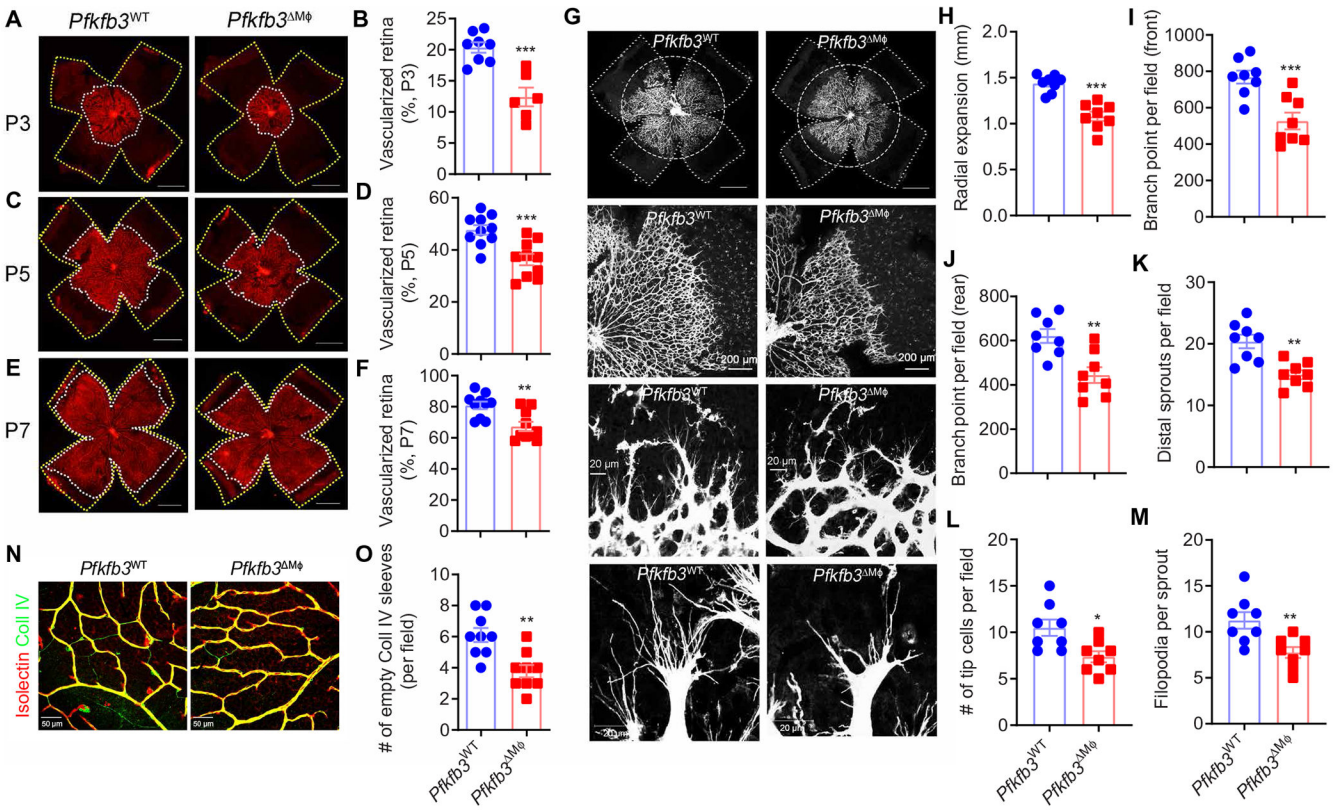

Fig. 2. Myeloid cell glycolysis participates in developmental retinal angiogenesis.

(**A** to **F**) The development of retina vasculature of *Pfkfb3*^{WT} and *Pfkfb3*$^{\Delta M\phi}$ mice at P3 (A), P5 (C), and P7 (E) in RA was visualized by isolectin B4 staining in whole-mount retinas. Vascularized areas and whole retinal surface are shown by white and yellow dotted lines, respectively. Quantification of the superficial vascularized areas of retinas at P3 (n = 6 to 8) (B), P5 (n = 10) (D), and P7 (n = 10) (F) as a percentage of the whole retinal area. (**G** to **M**) Isolectin B4 staining of vascular network in the P5 retinas of the indicated genotypes. Dashed lines depict the size of retina, and circles depict the size of vascular outgrowth from a representative *Pfkfb3*$^{\Delta M\phi}$ retina for comparison. (H) Quantification of retinal vascular outgrowth showing that myeloid-specific *Pfkfb3* KO (*Pfkfb3*$^{\Delta M\phi}$) reduces radial expansion (n = 8). (I to J) Quantification of the number of branch points at the front (I) or rear (J) in the retinal vasculature of *Pfkfb3*$^{\Delta M\phi}$ mice (n = 8). (K to M) Quantification of distal sprout number (K), tip cell number (L), and filopodia number per sprout (M). Scale bars, 1000 μm. (n = 8). (**N**) Retinas from P21 pups were costained with isolectin B4 and collagen IV (Coll IV) in RA *Pfkfb3*^{WT} and *Pfkfb3*$^{\Delta M\phi}$ retinas. (**O**) Quantification of the number of Coll IV^{+} isolectin^{-} sleeves (n = 9). Data are means ± SEM. *P < 0.05, **P < 0.01, and ***P < 0.001 by Student's t test.

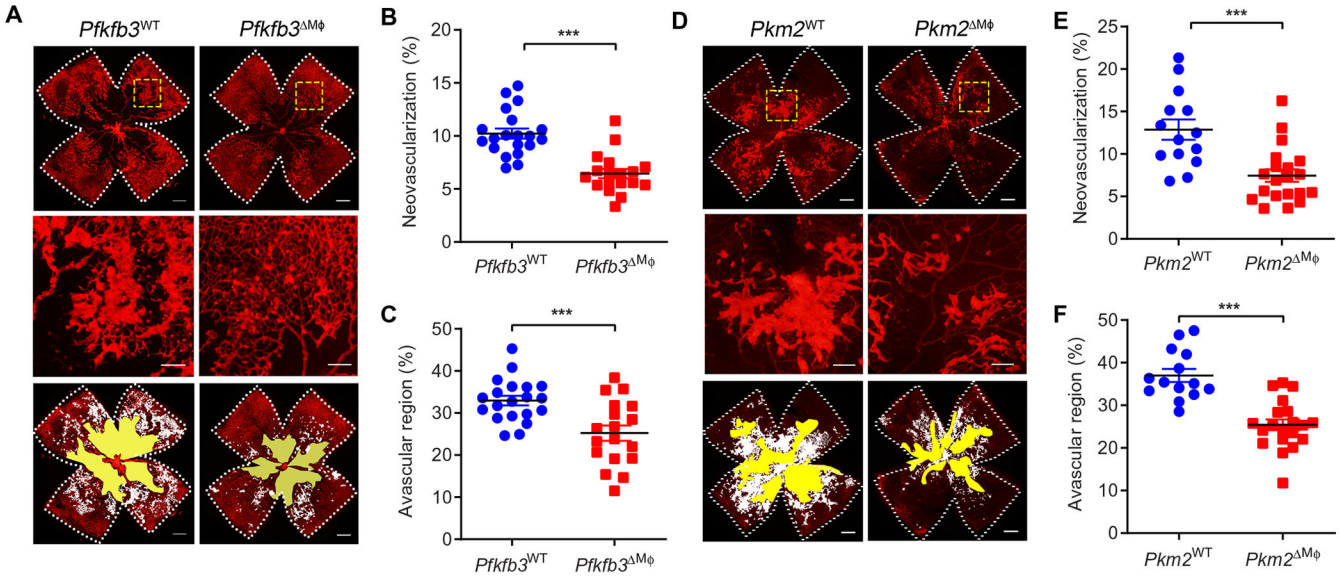

Fig. 3. *Pfkfb3* or *Pkm2* deficiency in myeloid cells delays pathological ocular angiogenesis.

(**A** and **D**) Representative retinal whole mounts from P17-OIR retinas of the indicated genotypes stained with isolectin B4 (red) with areas of vaso-obliteration (VO) and NV highlighted (white). Two selected retinal areas (yellow box) were enlarged to show pathological neovessels. Quantification of pathological NV (**B** and **E**) and VO (**C** and **F**) in OIR retinas was expressed as percentage of total retinal areas. $n = 18$ to 20 retinas for (A) to (C); $n = 14$ to 20 retinas for (D) to (F); Scale bars, 500 μm for original images and 200 μm for enlarged images. Data are means ± SEM. ***$P < 0.001$ by Student's t test.

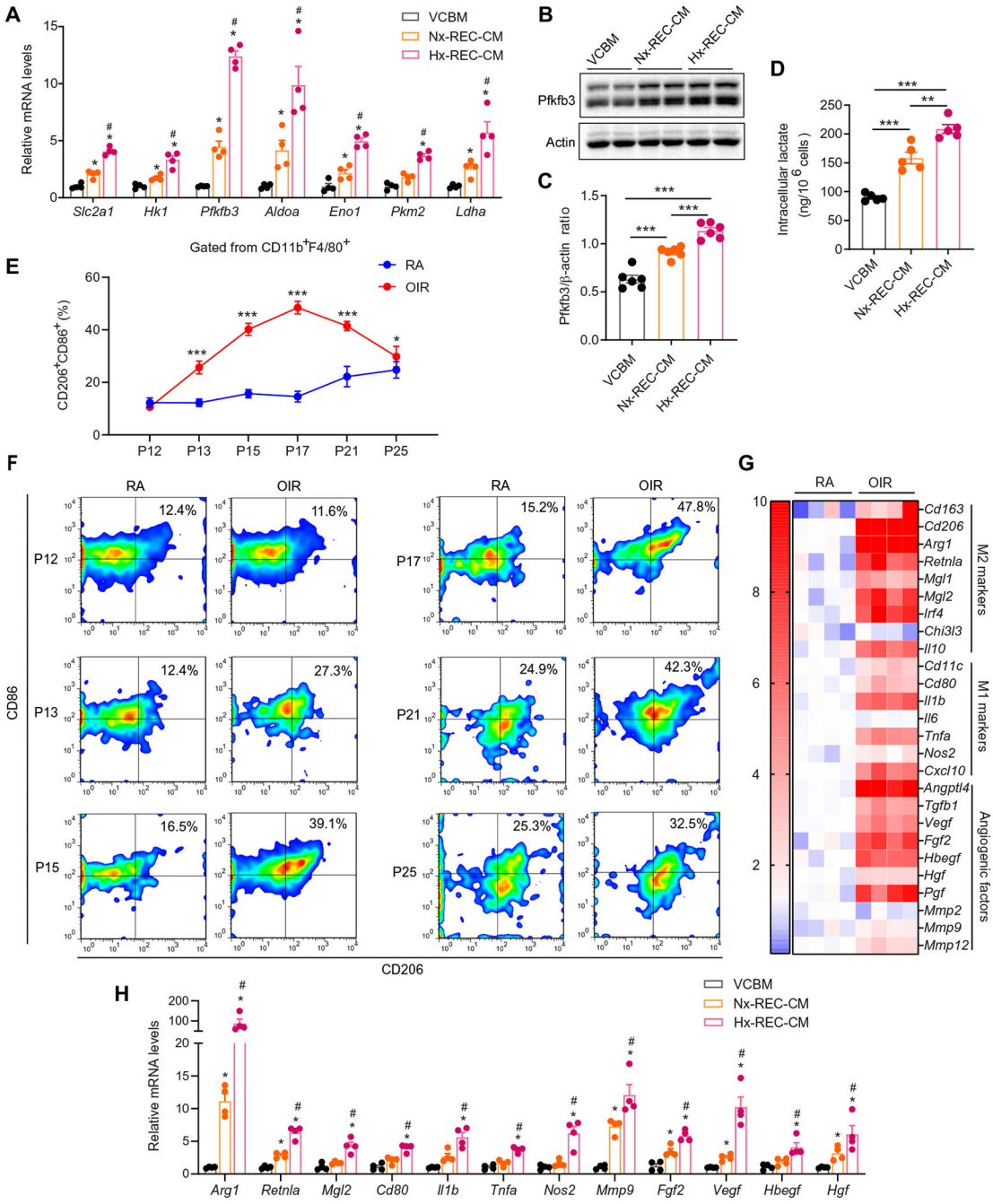

Fig. 4. EC-secreting soluble factor(s) induce macrophage glycolysis and polarize cells to mixed M1/M2-like macrophages.

(**A**) qRT-PCR analysis of the mRNA expression of glycolytic genes in BMDMs exposed to VCBM, Nx-REC-CM, or Hx-REC-CM for 12 hours ($n = 4$). *$P < 0.05$ versus VCBM. (**B** and **C**) Western blot analysis of Pfkfb3 protein expression in BMDMs exposed to VCBM, Nx-REC-CM, or Hx-REC-CM for 6 hours ($n = 6$). (**D**) The amount of intracellular lactate of BMDMs exposed to VCBM, Nx-REC-CM, or Hx-REC-CM for 12 hours. $n = 5$. **$P < 0.01$; ***$P < 0.001$. (**E** and **F**) Flow cytometry analysis of mixed M1/M2-like macrophages

(CD11b$^+$, F4/80$^+$, CD86$^+$, and CD206$^+$) in the retinas of RA and OIR mice at different time points from P12 to P25 $n = 4$). *$P < 0.001$ and ***$P < 0.001$ versus RA. Data are means ± SD. (**G**) Heatmap displaying the fold changes of gene expression detected by qRT-PCR in macrophages/microglia isolated from RA or OIR retinas in WT mice at P17 ($n = 4$). (**H**) qRT-PCR analysis of gene expression in BMDMs exposed to VCBM, Nx-REC-CM, or Hx-REC-CM for 12 hours ($n = 4$). *$P < 0.05$ versus VCBM; #$P < 0.05$ versus Nx-REC-CM. Data are means ± SEM. P value determined by one-way [for (A), (C), (D), and (H)] or two-way [for (E)] ANOVA followed by Bonferroni test.

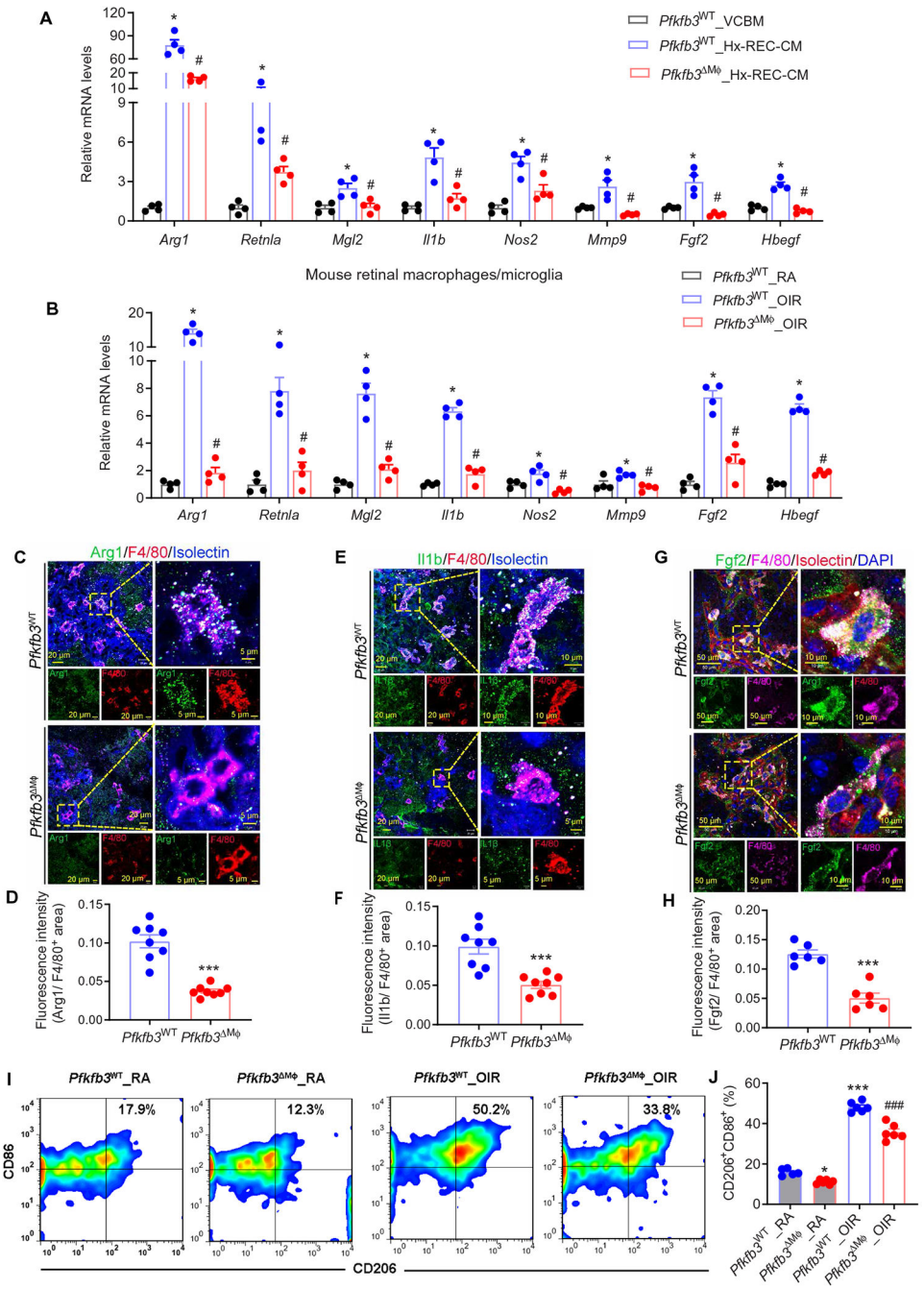

Fig. 5. Macrophage glycolysis induces macrophage activation.

(**A**) qRT-PCR analysis of gene expression in *Pfkfb3*^{WT} or *Pfkfb3*$^{\Delta M\phi}$ BMDMs exposed to VCBM or Hx-REC-CM for 12 hours ($n = 4$). *$P < 0.05$ versus VCBM_*Pfkfb3*^{WT}; #$P < 0.05$ versus Hx-REC-CM_*Pfkfb3*^{WT}. (**B**) qRT-PCR analysis of gene expression in macrophages/microglia isolated from RA or OIR retinas in *Pfkfb3*^{WT} or *Pfkfb3*$^{\Delta M\phi}$ mice at P17 ($n = 4$). *$P < 0.05$ versus *Pfkfb3*^{WT}_RA; #$P < 0.05$ versus *Pfkfb3*^{WT}_OIR. (**C** to **H**) Mutiple IHC of Arg1 (C), Il1β (D), Fgf2 (G), F4/80, and isolectin on the sections of P17 OIR retinas ($n = 6$ to 8). Fluorescence intensity of Arg1 (D), Il1β (F), and Fgf2 (H) staining was calculated by

ImageJ software. ***$P < 0.001$ versus *Pfkfb3*^{WT}. (**I** to **J**) Representative flow cytometric plots of retinal CD11b^{+}F4/80^{+} cells showed CD86^{+}CD206^{+} fractions in the retinas of RA and OIR mice at P17 (I) and comparisons of CD86^{+}CD206^{+} fractions between genotypes (J) ($n = 5$ to 6). *$P < 0.05$; ***$P < 0.001$ versus *Pfkfb3*^{WT}_RA; ###$P < 0.001$ versus *Pfkfb3*^{WT}_OIR. Data are means ± SEM. *P* value determined by Student's *t* test [for (D), (F), and (H)] and one-way ANOVA followed by Bonferroni test [for (A), (B), and (J)].

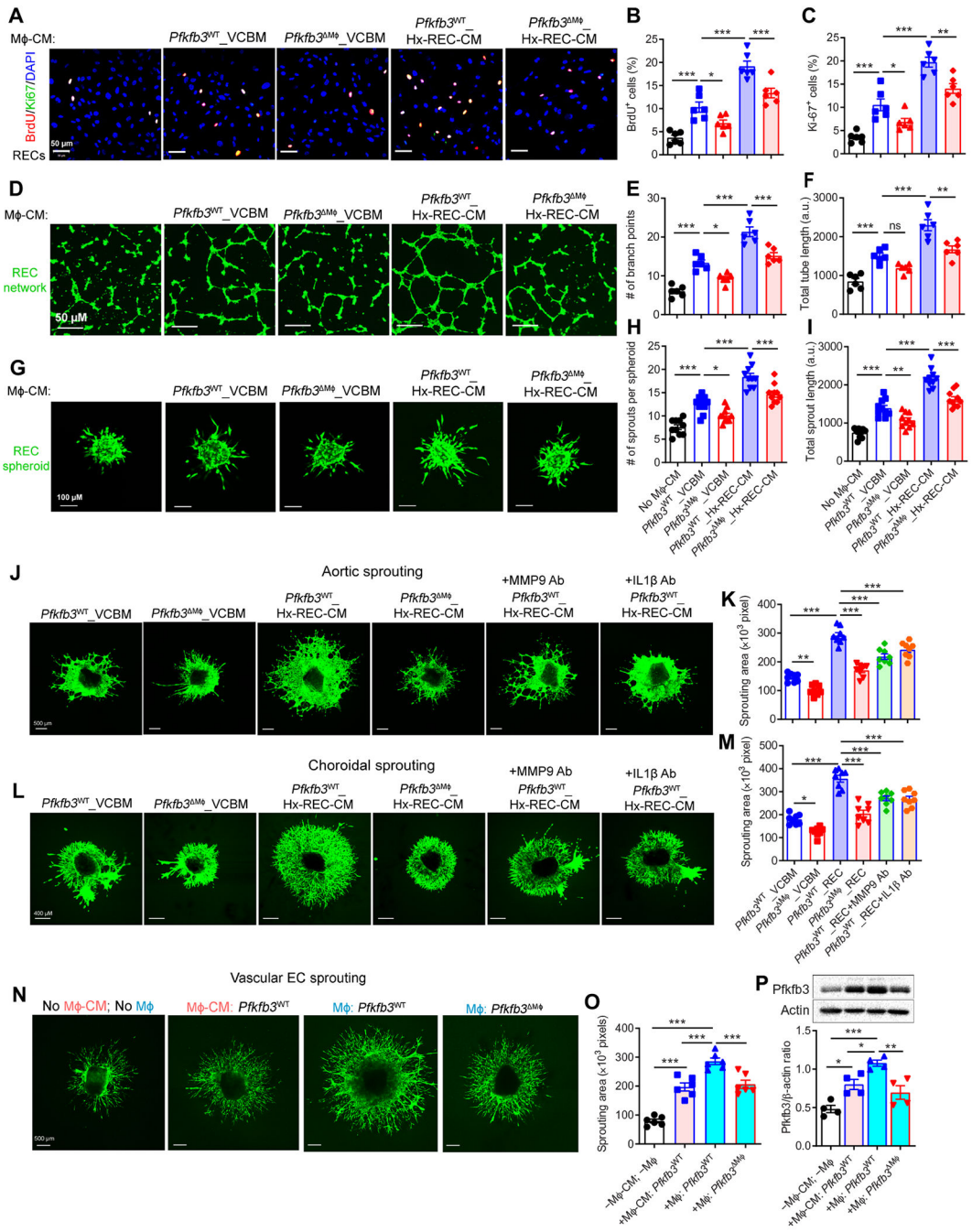

Fig. 6. Reprogrammed endogenous glycolysis in macrophages supports their angiogenic activity.

(**A** to **C**) Ki-67 and BrdU staining of human RECs. Human RECs were exposed to conditioned medium (CM) from *Pfkfb3*^{WT} or *Pfkfb3*$^{\Delta M\phi}$ BMDMs pretreated with control medium (VCBM) or hypoxic REC-CM (Hx-REC-CM) for 12 hours. $n = 6$. (**D** to **I**) Human RECs were cultured in collagen gel to grow into three-dimensional multicellular spheroids, or on a two-dimensional matrix to form a tube network in the presence or absence of CM from *Pfkfb3*^{WT} or *Pfkfb3*$^{\Delta M\phi}$ BMDMs pretreated with VCBM or Hx-REC-CM. Representative fluorescence photographs of angiogenic tube formation after culturing for 8

hours in matrix (D). Scale bars, 50 μm. Cumulative tube length quantified using the ImageJ software (E) and branch points calculated from five experiments in each case ($n = 6$) (F). Representative images of spheroidal sprouting after culturing for 24 hours in collagen matrix (G). Scale bars, 100 μm. Morphometric quantification of spheroid sprouting by calculating the number of sprouts per spheroid (H), as well as total sprout length (I). $n = 10$ per group. n is number of spheroids quantified. a.u., arbitrary units. (**J** to **M**) Representative images of sprouting aortic rings (J) and choroids (L) exposed to CM from *Pfkfb3*^{WT} or *Pfkfb3*$^{\Delta M\phi}$ BMDMs pretreated with VCBM or Hx-REC-CM for 12 hours. Sprouting areas were quantified (K and M). (**N**) Sprouting aortic rings were exposed to CM from *Pfkfb3*^{WT} BMDMs, or cocultured with BMDMs from *Pfkfb3*^{WT} or *Pfkfb3*$^{\Delta M\phi}$ in Transwells. Representative images of sprouting aortic rings at day 8 ($n = 6$ per group). (**O**) Sprouting areas were quantified. Scale bars, 500 μm. (**P**) Western blot analysis of Pfkfb3 protein expression in mouse aortic ECs collected from (N). $n = 4$. Data are means ± SEM. $^{*}P < 0.05$; $^{**}P < 0.01$; $^{***}P < 0.001$, by one-way ANOVA followed by Bonferroni test.

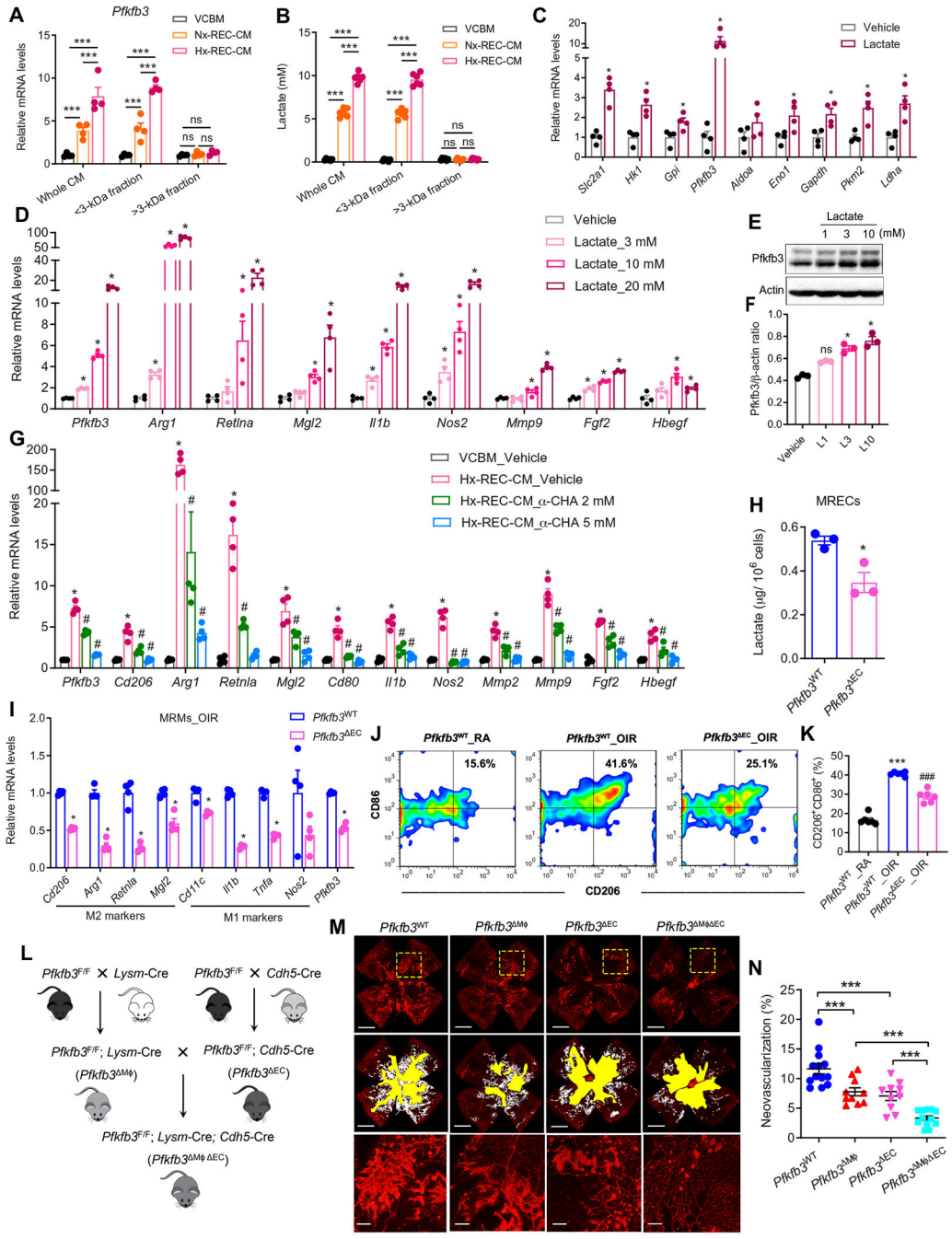

Fig. 7. REC-secreting lactate is sufficient to induce macrophage glycolysis and activation.

(**A**) VCBM, Nx-REC-CM, or Hx-REC-CM were used unfractionated (whole) or as >3-or <3-kDa fractions to stimulate BMDMs for 12 hours as follows. qRT-PCR analysis of the Mrna expression of *Pfkfb3* in BMDMs. $n = 4$. ***$P < 0.001$ versus VCBM. ns, not significant. (**B**) Lactate concentration in medium from (A). $n = 6$. ***$P < 0.001$. (**C**) qRT-PCR analysis of the mRNA expression of glycolytic genes in BMDMs treated with 10 mM lactate for 12 hours ($n = 4$). *$P < 0.05$ versus vehicle. (**D**) qRT-PCR analysis of gene expression in BMDMs stimulated with a concentration gradient (3 to 20 mM) of lactate for

12 hours. $n = 4$. *$P < 0.05$ versus vehicle. (**E** and **F**) Western blot analysis and quantification of Pfkfb3 protein expression in BMDMs stimulated with lactate for indicated concentrations for 12 hours. $n = 3$. *$P < 0.05$ versus vehicle. (**G**) qRT-PCR analysis of gene expression in BMDMs exposed to VCBM or Hx-REC-CM for 12 hours, with or without α-cyano-4-hydroxycinnamic acid (α-CHA) (2 to 5 mM) treatment ($n = 4$). *$P < 0.05$ versus VCBM_Vehicle; #$P < 0.05$ versus Hx-REC-CM_Vehicle. (**H**) The amount of intracellular lactate of retinal ECs (MRECs) isolated from OIR *Pfkfb3*^{WT} or *Pfkfb3*$^{\Delta M\phi}$ mice at P17. *$P < 0.05$ versus *Pfkfb3*^{WT}. (**I**) qRT-PCR analysis of gene expression in mouse retinal macrophages/microglia isolated from OIR *Pfkfb3*^{WT} or *Pfkfb3*$^{\Delta EC}$ mice at P17 ($n = 4$). *$P < 0.05$ versus *Pfkfb3*^{WT}. (**J** and **K**) Representative flow cytometric plots of retinal CD11b^{+}F4/80^{+} cells showed CD86^{+}CD206^{+} fractions in the retinas of RA and OIR mice at P17 (J) and comparisons of CD86^{+}CD206^{+} fractions between genotypes (K) ($n = 6$). ***$P < 0.001$ versus *Pfkfb3*^{WT}_RA; ###$P < 0.001$ versus *Pfkfb3*^{WT}_OIR. (**L**) Schematic illustration of the generation of myeloid and EC-specific *Pfkfb3* double-KO (*Pfkfb3*$^{\Delta M\phi\Delta EC}$) mice. (**M**) Representative retinal whole mounts from P17-OIR retinas of the indicated genotypes stained with isolectin B4 (red) with areas of NV highlighted (white). Two selected retinal areas (yellow box) were enlarged to show pathological neovessels. Quantification of pathological NV (**N**) in OIR retinas was expressed as percentage of total retinal areas. $n = 10$ to 13; Scale bars, 1000 μm for original images and 200 μm for enlarged images. ***$P < 0.001$. Data are means ± SEM. P value by Student's t test [for (C), (H), and (I)] and one-way ANOVA followed by Bonferroni test [for (A), (B), (D), (F), (G), (K), and (N)].

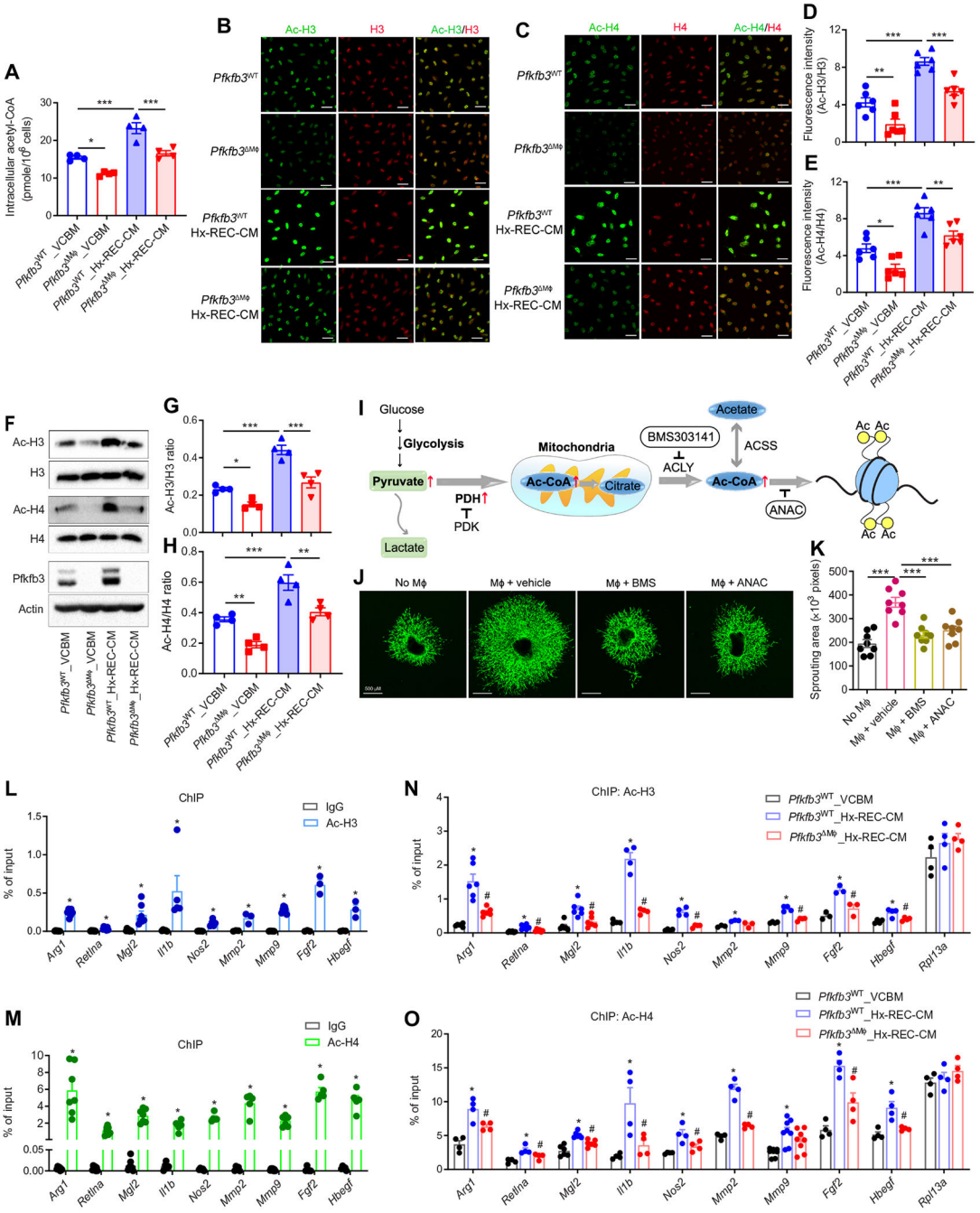

Fig. 8. Glycolytic metabolites mediate REC-induced macrophage activation via histone acetylation.

BMDMs from *Pfkfb3*^{WT} or *Pfkfb3*$^{\Delta M\phi}$ mice were exposed to VCBM or Hx-REC-CM for 6 hours. (**A**) The amount of acetyl-CoA (coenzyme A) in BMDMs. $n = 4$. (**B** to **E**) Immunofluorescent staining of acetylated H3 (Ac-H3, green) (B) and total H3 (red), acetylated H4 (Ac-H4, green) (C) and total H4 (red) in BMDMs, respectively. (D and E) Fluorescence intensity was calculated by ImageJ software. $n = 6$. (**F** to **H**) Western blot analysis of Ac-H3, Ac-H4, H3, H4, Pfkfb3, and β-actin in BMDMs, with quantification. $n =$

4. (**I**) Schematic of metabolic regulation of histone acetylation in macrophages. PDH, pyruvate dehydrogenase. PDK, pyruvate dehydrogenase kinase. (**J** to **K**) BMDMs were pretreated with BMS303141 (10 μM) or anacardic acid (ANAC) (20 μM) for 24 hours, before being cocultured with choroid explants in transwells. (J) Representative images of choroid explant sprouts at day 8. (K) Sprouting areas were quantified ($n = 8$). (**L** to **O**) ChIP of Ac-H3 (L and N) and Ac-H4 (M and O) on gene promoters in BMDMs exposed to VCBM or Hx-REC-CM for 6 hours. Enrichment of the indicated gene promoters was assessed by qRT-PCR. $n = 3$ to 8. $^{*}P < 0.05$ versus immunoglobulin G (IgG) (L and M). $^{*}P < 0.05$ versus VCBM_*Pfkfb3*^{WT}. $^{\#}P < 0.05$ versus *Pfkfb3*^{WT}_Hx-REC-CM (N and O). Data are means ± SEM. $^{*}P < 0.05$; $^{**}P < 0.01$; $^{***}P < 0.001$. *P* value determined by Student's *t* test [for (L) and (M)] and one-way ANOVA followed by Bonferroni test [for (A), (D), (E), (G), (H), (K), (N), and (O)].